PCCP

Accepted Manuscript

ROYAL SOCIETY OF CHEMISTRY

www.rsc.org/pccp

PCCP

RSCPublishing

ARTICLE

High performance photoelectrochemical hydrogen generation and solar cells with a double type II heterojunction†

Cite this: DOI: 10.1039/x0xx00000x

Received 00th January 2012,
Accepted 00th January 2012

DOI: 10.1039/x0xx00000x

www.rsc.org/

Lai-Hung Lai,[a] Widianta Gomulya,[‡a] Loredana Protesescu,[‡b,c] Maksym V. Kovalenko[b,c] and Maria A. Loi[*a]

We report on the fabrication of CdSe quantum dot (QD) sensitized electrodes by direct adsorption of colloidal QDs on mesoporous TiO_2 followed by 3-mercaptopropionic acid (MPA) ligands exchange. High efficiency photoelectrochemical hydrogen generation is demonstrated by mean of these electrodes. The deposition of ZnS on the TiO_2/CdSe further improves the external quantum efficiency from 63% to 85% at 440nm under -0.5 V vs SCE. With the same photoelectrodes, solar cells with internal quantum efficiency approaching 100% are fabricated. The ZnS deposition increases the photocurrent and chemical stability of the electrodes. Investigation of the carrier dynamics of the solar cells shows that ZnS enhances the exciton separation rate in CdSe nanocrystals, which we ascribe to the formation of a type II heterojunction between ZnS and CdSe QDs. This finding is confirmed by the dynamics of the CdSe photoluminescence, which in the presence of ZnS becomes noticeably faster.

1. Introduction

Photocatalytic water splitting was first demonstrated by Honda and Fujishima by employing TiO_2 as a photoanode and Pt as a cathode in 1972.[1] Owing to the wide band gap characteristic of TiO_2, the energy conversion efficiency was rather low. In the last 40 years myriads of researchers tried to improve the efficiency of water splitting by different approaches. For example, N-doped TiO_2 photoanodes were used to extend the absorption towards the visible region[2] but the doping induce defects,[3] which are the origin of performance degradation. Another route, which has been largely investigated, is to harvest the visible light by introducing narrow band gap semiconductors as absorbers on mesoporous TiO_2.[4-8]

Narrow band gap nanoparticles seems ideal due to their tunable band gap, high extinction coefficient and stability. Recently, the use of semiconducting nanoparticles mostly growth by chemical bath deposition (CBD) or similar techniques has emerged as a viable and simple method to enhance the performance of photoelectrochemical H_2 generation.[4, 5, 7, 9-11] For instance, CdSe nanoparticles deposited by atomic layer deposition and ion exchange reaction (ALDIER) on electrodes of TiO_2 inverse opals show a remarkable current density of about 15.7 $mA \cdot cm^{-2}$ for photoelectrochemical H_2 generation in three electrodes configuration.[5] Mesoporous TiO_2 electrodes sensitized with PbS/CdS deposited by successive ionic layer adsorption and reaction (SILAR) show current density of 6 $mA \cdot cm^{-2}$ in two electrodes configuration.[7]

Compared to the great number of works, which use CBD or similar in-situ growth techniques, a limited number of articles report photocatalytic water splitting devices sensitized by ex-situ synthesized quantum dots of controlled size and shape (monodispersed colloidal quantum dots). ZnO nanowires electrodes sensitized with CdTe colloidal nanocrystals linked with MPA showed 2 $mA \cdot cm^{-2}$ in non-sacrificial electrolyte.[12] Photoelectrodes made by InP nanocrystals crosslinked by 1,4-benzenedithiol (BDT) are reported to show photocatalytic water reduction properties.[13]

Looking at the homologous solar cell devices, the efficiency of devices fabricated by CBD was significantly enhanced in recent years. $CdSe_{0.45}Te_{0.55}$ alloyed nanoparticles sensitized solar cells exhibiting record power conversion efficiency of 6.36%.[14] CdSe and CdS co-sensitized nanoparticles[4, 6, 9, 15-17] and PbS nanoparticles[8, 18] fabricated by CBD and SILAR were used as absorbers for sensitized solar cells owing to their narrower band gaps and appropriate band alignment with respect to TiO_2 and ZnO. However, the in-situ deposition methods give polydispersed nanoparticles, which due to the variation of the bandgap may give rise to charge trapping. Ex-situ nanocrystals sensitization, such as electrophoretic deposition[19-21] and direct adsorption[10] on metal oxide, should in principle allows for a better-controlled energy landscape.

Between the many heterostructures proposed, CdSe and CdS sensitized electrodes are the ones more systematically studied.[15, 21, 22] In particular a CdS interlayer deposited between TiO_2 and CdSe has been found to help charge separation.[15] The alignment of the Fermi level after the contact between CdS and CdSe results in downward and upward shift of CdS and CdSe band gap, respectively. This has been reported to allow the formation of a type II heterostructure, which drives the charge separation upon illumination.[15, 22]

Here we report on the fabrication of efficient photocatalytic electrodes composed by TiO_2 and colloidal CdSe QDs. The CdSe quantum dot (QD) sensitized electrodes are made by direct adsorption of colloidal QDs on mesoporous TiO_2 followed by MPA ligands exchange. External quantum efficiency (EQE) of 63% at 440 nm under -0.5 V vs SCE is obtained. Significant improvement of the quantum efficiency, EQE from 63% to 85% at 440nm under -0.5 V vs SCE, is achieved upon deposition of ZnS on the electrodes.

By using the same semiconductor heterostructure, solar cells with internal quantum efficiency approaching 100% are obtained. The photophysics and carrier transport dynamics of CdSe QDs sensitized electrodes in photoelectrochemical hydrogen generation and solar cells are studied to elucidate the device functioning mechanism. Time-resolved spectroscopy shows a reduction of the exciton lifetime for the samples coated with ZnS (from ~11 ps (τ_1) and ~150 ps (τ_2) for the TiO_2/CdSe to ~8 ps (τ_1) and ~41 ps (τ_2) for the TiO_2/CdSe/ZnS(2L)) demonstrating the formation of a type II heterojunction between ZnS and the CdSe QDs. These data are confirmed by impedance spectroscopy, which shows that ZnS enhances the charge injection (separation) efficiency.

2. Experimental Section

CdSe Nanocrystal Synthesis.

The synthesis of CdSe NCs was adopted from Ref. [23] To prepare Cd-myristate precursor, Cadmium nitrate (1.542 g, 5 mmol, in 150 mL methanol) was added dropwise to sodium hydroxide (0.6 g, 15 mmol) and myristic acid (3.42 g, 15 mmol) in methanol (500 mL). The resulting white precipitate was washed with methanol three times, and then dried at ~60°C under vacuum overnight. CdSe NCs were then synthesized by combining cadmium myristate 1.132 g (2 mmol), SeO_2 (2 mmol) and ODE (128 mL) in a 500 mL three-neck flask. The resulting mixture was degassed under vacuum (~50 mTorr, 10 min) at room temperature. Under argon flow and with stirring, the mixture was heated to the reaction temperature (240 °C) at a rate of 20 °C/min. After 3 minutes at 240 °C, 4 mL of oleic acid was injected and the mixture was cooled down to RT. ODE was distilled from crude solution at 155°C under vacuum until 20 mL of solvent was left in the flask. The particles were washed 3 times with hexane as solvent and ethanol as nonsolvent. A quantum yield of about 1.7% is measured for CdSe/oleate (reference Rhodamine 26).

Preparation of the Photoanode.

The FTO substrates (Sigma-Aldrich, sheet resistivity ~7 Ω/sq) were cleaned with soap water and sonicated in deionized (DI) water, aceton and isopropyl alcohol in ultrasonic bath for 10 min for each cleaning step. A thin and compact TiO_2 layer was coated on FTO by immersing the substrates into 40mM $TiCl_4$ at 70°C for 30 min. Mesoporous TiO_2 films were prepared with TiO_2 paste (Solaronix D/SP) by doctor blading. Samples were annealed at 450°C for 30 min to remove organics and make the film porous. Another thin TiO_2 layer was formed using $TiCl_4$ as the procedure before. Further annealing process was done at 450°C for 30 min. The final TiO_2 thickness is ~4 μm measured by a step profiler (Veeco DEKTAK 150). The QDs colloidal solution (5 mg/ml) was drop-casted on the TiO_2 photoelectrodes and let drying for 20min. After colloidal deposition samples were washed with hexane to remove residual QDs not absorbed on the TiO_2 surface. Ligand exchange was done by immersing QDs-sensitized TiO_2 into 10% (v/v) 3-mercaptopropionic acid (3-MPA)(99%, Sigma-Aldrich) in methanol solution for 10 min. Samples were again washed with methanol followed by annealing at 90°C for 10min to remove the solvent. ZnS was deposited by two SILAR half cycle reactions. First, samples were dipped into 0.1M aqueous $Zn(NO_3)_2$ ($Zn(NO_3)_2.6H_2O$, 98%, Sigma-Aldrich) for 1 min, followed by rinsing with DI water and drying with a N_2 gun. For the second cycle, samples were dipped into 0.1M aqueous Na_2S ($Na_2S.9H_2O$, 98%, Sigma-Aldrich) for 1 min, followed by rinsing with DI water and drying with a N_2 gun. These two half cycle reactions are named one SILAR layer.

Assembly of CdSe QDSSCs.

The photoanode (active area is $1cm^2$) and the Cu_xS counter electrode were sandwiched together with a Teflon spacer (~2 mm thickness), the 2 M Na_2S/2 M S in H_2O-MeOH (7:3, v/v) polysulfide electrolyte was injected into the cell.

Assembly of Photoelectrochemical cell.

The three electrodes electrochemical cell is composed of QD sensitized electrode, Pt counter electrode, saturated calomel electrode (SCE) and 0.35M Na_2SO_3/0.25 M Na_2S aqueous electrolyte.

Characterization.

Absorbance, reflectance and transmittance are measured by UV-3600 UV-Vis-NIR spectrophotometer (Shimadzu Scientific Instruments) equipped with 3 detectors (PMT, InGaAs and PbS) and an integrating sphere. The ZnS thickness is measured by Ellipsometer (V-VASE, J. A. Woollam Co., Inc.), in which the ZnS was deposited on Si substrates with 300 nm SiO_2 on the top. I-V curves were measured by SP-200, Bio-Logic potentiostat equipped with electrochemical impedance spectroscopy analyzer. Solar cells measurements are performed under 100 mW/cm^2 AM 1.5G conditions obtained with a solar simulator (SF150 class A, Sciencetech) calibrated by a Si reference cell (SRC-1000-RTD-QZ, VLSI Standards Incorporated). External quantum efficiencies (EQE) measurements are performed with a 250 W quartz tungsten halogen lamp (6334NS, Newport with lamp housing 67009, Newport), wavelength selection is obtained with a set of band pass filters (Thorlabs) with full width half max (FWHM)= 10 ±

2 nm from 400 nm to 740 nm. PD300 (Ophir Optics) is used as calibrated photodiodes. Impedance spectroscopy was performed by applying a 15 mV ac signal over the frequency range 1 MHz-50 mHz at open circuit voltage under different light intensity (from AM 1.5, 1 sun to 0.1 sun).

Photoluminescence measurements were performed by exciting the samples at 380 nm by the second harmonic of a mode-locked Ti:Sapphire laser delivering pulses of 150 fs and repetition frequency of 76 MHz. The steady state PL was recorded using a Si CCD detector, while the time-resolved PL was recorded by a Hamamatsu streak camera working in synchroscan mode. All PL spectra are corrected for the spectral response of the setup. The measurements are done in transmission mode.

3. Results and Discussion

Figure 1 reports the structures of the CdSe QD-sensitized electrodes for solar cells (Figure 1(a)) and photocatalytic water splitting (Figure 1(b)). The solar cells are composed by the mesoporous TiO_2 sensitized with QDs, the polysulfide electrolyte, and a Cu_xS counter electrode. The photocatalytic water splitting device is composed by a QDs sensitized mesoporous TiO_2 photoelectrode (detail in Figure 1b), the electrolyte, a saturated calomel electrode (SCE) as reference, and a Pt coil as counter electrode. In both devices ZnS is deposited on top of the QDs (Figure 1b).

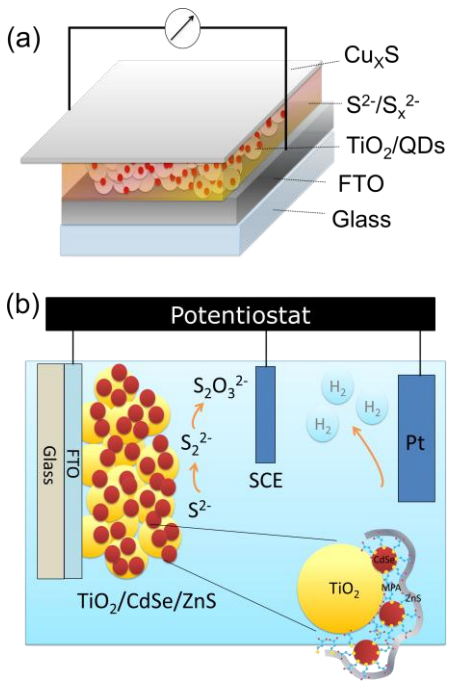

Figure 1. Schematic diagrams illustrating (a) the QDSSCs: QD-sensitized mesoporous TiO_2 electrode, polysulfide electrolyte, and Cu_xS counter electrode. (b) The photoelectrochemical cells: QDs sensitized mesoporous TiO_2 photoelectrodes, electrolyte, reference electrode, and counter electrode. The microscopic structure of the electrodes is shown in (b).

The electrochemical reactions for both the water splitting and the solar cells devices are reported in the supporting information. The main difference between the two device structures is the electrolyte. The polysulfide electrolyte (Na_2S/S) is used for QDSSC and the sacrificial electrolyte (Na_2S/Na_2SO_3) is used for the photoelectrochemical device.

The J-V characteristics and EQE of the CdSe QD-sensitized solar cells with different number of ZnS layers are shown in Figure 2a and 2b, respectively. The CdSe QDs sensitized electrodes with on top 5L ZnS coating made with the SILAR procedure show 1.6 times higher photocurrent and 6.3% higher photovoltage than the samples without ZnS coating. The energy conversion efficiency enhanced from 1.21% to 1.93% (2L ZnS) and 2.04% (5L ZnS) upon ZnS coating. All the device parameters, obtained as averaged value of the fabricated devices are reported in Table 1.

Table 1. Summary of Device Parameters. The standard deviations are reported in the round brackets.

Sample	I_{sc} (mA/cm^2)	V_{oc} (V)	FF	Efficiency (%)
0L ZnS	4.81(0.36)	-0.48(0.01)	0.53(0.01)	1.21(0.15)
2L ZnS	6.65(0.04)	-0.52(0.01)	0.56(0.02)	1.93(0.11)
5L ZnS	7.52(0.44)	-0.51(0.01)	0.53(0.02)	2.04(0.15)

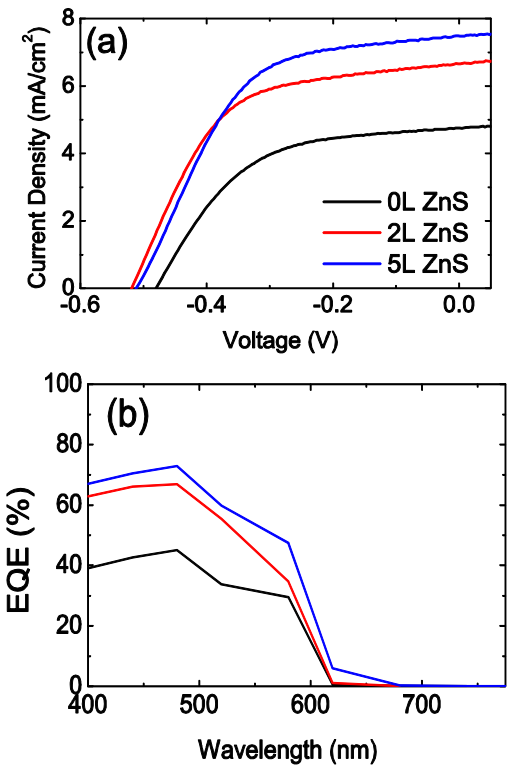

Figure 2. (a) J-V curves of CdSe QD-sensitized solar cell with 0, 2 and 5 layers of ZnS measured under 100mW/cm^2 at AM1.5. (b) EQE of CdSe QD-sensitized solar cells as in panel (a).

From the EQE data and the reflection and transmission measurements performed on the devices (Figure S3 of the supplementary information) we derived the internal quantum efficiency (IQE) of our solar cells (Figure 3). Figure 3 shows that 2L ZnS coating is enough to increase IQE from 61% to 100% at 440nm. Nevertheless, the highest power conversion efficiency of the devices is obtained with 5L ZnS, which seems to be due to the extended low energy tail of the EQE spectra of the sample. Similar red-shift is observed in the absorption measurements which are reported in Figure S4 of the supplementary information section.

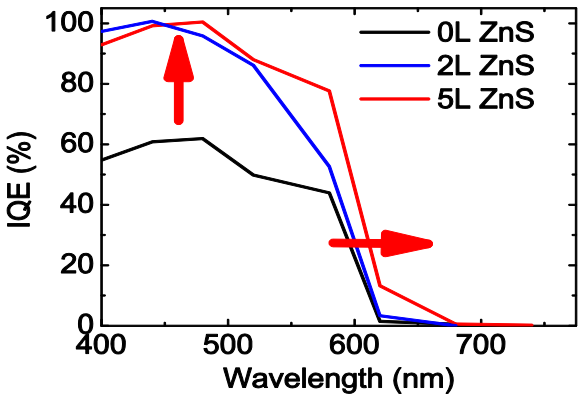

Figure 3. Internal quantum efficiency of QDSSC with and without ZnS coating.

A similar effect upon ZnS deposition was reported by other authors[24] and explained as due to the larger delocalization of the carriers wave function in presence of ZnS. We believe that the reason for this phenomenon should be found in interfacial effects occurring between CdSe and ZnS and in particular in the heterostructure formation between the two semiconductors, which will be discussed in detail later.

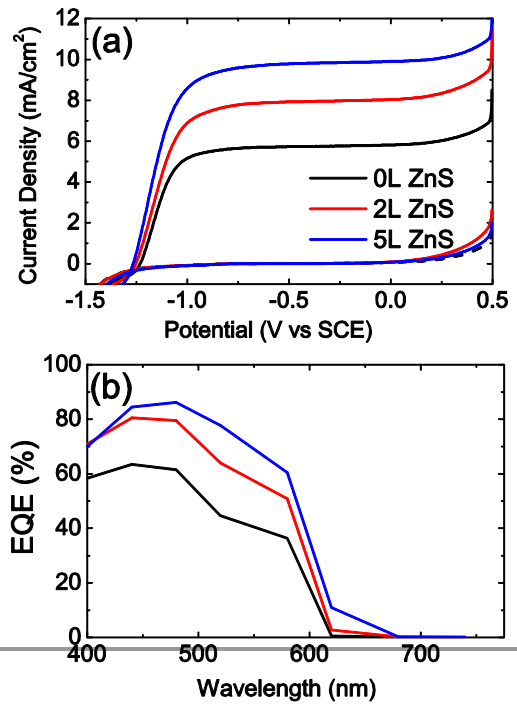

Figure 4. (a) J-V curves of CdSe QD sensitized electrodes in 0.25M Na_2S and 0.35M Na_2SO_3 aqueous electrolyte measured under 100mW/cm^2 at AM1.5. **(b)** EQE of CdSe QD sensitized electrodes measured at -0.5V vs. SCE.

The same photoelectrodes are used to demonstrate photoelectrochemical hydrogen generation. The main difference respects to the QDSSC are the electrolyte and counter electrodes as shown in Figure 1(b). The J-V characteristics and EQE of the photocatalytic CdSe QD-sensitized electrodes for water splitting are shown in Figure 4a and 4b, respectively. The three electrodes configuration is used to characterize the properties of the photoanodes. In this configuration the H_2 generation rate is proportional to the current density. Similarly to what shown by the QDSSC, the CdSe QD-sensitized electrodes with 2L and 5L ZnS coating show 1.38 and 1.7 times higher photocurrent at -0.5V vs SCE, respectively, compared to that without ZnS coating. Current density up to ~10 mA/cm^2 under -0.5 V vs SCE is achieved for CdSe QD-sensitized electrodes with 5L ZnS coating. The EQE spectra (Figure 4b) measured at -0.5V vs SCE shows significantly enhanced photocurrent from 63% till 84% at 480 nm wavelength, upon 5L ZnS deposition. Moreover, also here the onset of the EQE spectra shows, similarly to the solar cells, a broadening at around 620 nm. This broadening makes the photocurrent spectra resemble closely the absorption spectra of the electrodes shown in Figure S3b.

The stability of the photoelectrodes under continuous light illumination is shown in Figure 5, demonstrating that the ZnS coating is not only increasing the efficiency of the devices but also the photostability. The photocurrent of the pristine CdSe photoanode decays of 60% after 1 hr continuous illumination under AM 1.5 at 1 sun light intensity; while for the same electrode with 2L and 5L of ZnS coating, the photocurrent decays of 33% and 10%, respectively.

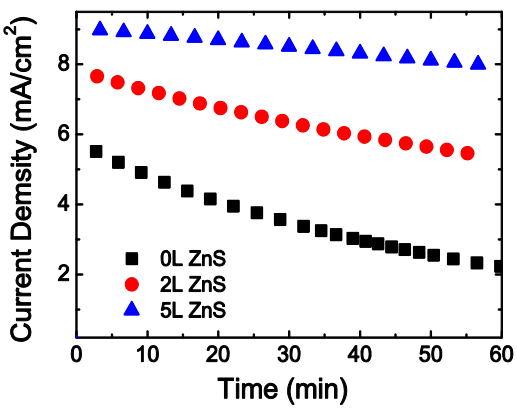

Figure 5. Time dependent current density of the CdSe QD-sensitized electrodes under continuous illumination with 100mW/cm2 and a bias of -0.5V vs SCE.

Many authors of the recent literature believe that ZnS coating acts as barrier, which suppresses the recombination of electrons (in either TiO_2 or CdSe) with the electrolyte; others reported that ZnS has the role to passivate defects at the quantum dot surface and to prevent photocorrosion.[24-28] To further investigate the working mechanism of ZnS coating in the colloidal quantum dot-sensitized electrodes using MPA as crosslinker, steady-state and time-resolved photoluminescence are measured.

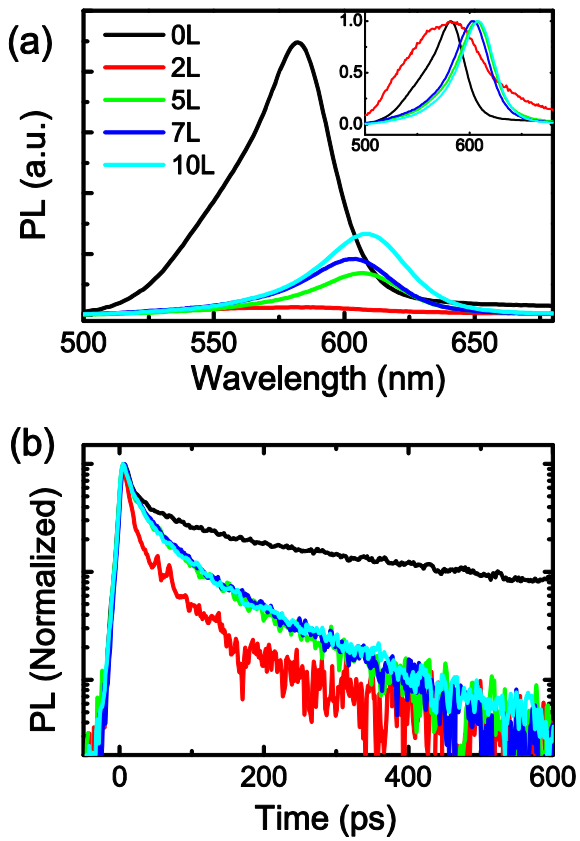

Figure 6. (a) Steady-state PL of the TiO_2/CdSe and TiO_2/CdSe/ZnS samples with different number of ZnS layers. Inset: PL spectra as in figure (a) normalized to the maximum of the intensity. (b) Time-resolved photoluminescence of CdSe QD sensitized electrodes coated with different layers of ZnS. (All measurements are performed in the absence of electrolyte).

Figure 6(a) shows the steady state PL spectra of the TiO_2/CdSe electrode with different amount of layers of ZnS. Upon deposition of 2L of ZnS, the photoluminescence signal is strongly quenched and becomes very broad (inset of figure 6(a)). The further deposition of ZnS layers on the same sample red-shift the photoluminescence signal (peak from 581 nm to 607 nm) while the intensity partially recoveres (Figure 6(a)). Time-resolved photoluminescence measurements allow gaining a clearer picture of the physics at the interface between CdSe and ZnS. Figure 6(b) shows the PL lifetimes of samples of TiO_2/CdSe and TiO_2/CdSe with on top 2, 5, 7 and 10 layers of ZnS. The lifetimes fitted with a bi-exponential function are ~11 ps (τ_1) and ~150 ps (τ_2) for the TiO_2/CdSe, quenched to ~8 ps (τ_1) and ~41 ps (τ_2) for the TiO_2/CdSe/ZnS (2L). With 5L of ZnS coating, the exciton lifetime increases to 12 ps (τ_1) and 67 ps (τ_2). The results of the fittings of the time-resolved PL are summarized in Table S2. It is worth noting that the measurements were performed in absence of the electrolyte on a single sample, on top of which subsequent layers of ZnS were deposited. The faster decay of the photoluminescence suggests the formation of a type II heterojunction between the CdSe QDs and ZnS as shown in the schematic in Figure 7b in which ZnS acts as hole transporting layer. In addition, PL measurements in samples in which ZnS (2L) is deposited between TiO_2 and CdSe were performed and compared with the reference samples composed by CdSe on TiO_2 and with the samples with ZnS on top of CdSe. The measurements reported in Figure S5 show an increase of the photoluminescence in the sample with the ZnS between TiO_2 and CdSe. These experiments provide further proof that CdSe/ZnS forms a type II heterostructure as shown in Figure 7b.

To explain how CdSe/ZnS can form a type II heterojunction (Figure 7b) even if in bulk forms a type I like heterojunction (Figure 7a), we need to look carefully at the macroscopic of our samples. Again, the QD-sensitized electrode is made by direct adsorption of CdSe QDs on mesoporous TiO_2 followed by 3-mercaptopropionic acid ligands exchange. The thiols and carboxylic acid groups have a preference to bind with Cd and TiO_2, respectively (Figure 7c). 3-mercaptopropionic acid is a molecular dipole on the CdSe QD surface, which shifts the relative band position of CdSe and ZnS.[29] It is supposed that the band energy is affected by both the Fermi level of ZnS and CdSe as well as the dipole of linkers.[30] In general CdSe nanocrystals have n-type property[31] and ZnS has been reported having both n-type and p-type properties depending on the stoichiometric ratio of Zn and S.[32] For the SILAR ZnS, the polarity is still not clear. As for the CdSe QD with thin layer (2L) of ZnS coating, the dipole dominates the band shifting, forming a type II heterojunction. However, with relative thick layer (5L) of ZnS coating, the Fermi level of ZnS causes the shifting of the band position, resulting in slightly enhanced light emission and exciton lifetime. The red shift of PL (and of the absorption) peak with the increasing of the number of layers of ZnS coating is ascribed to the weakening of the quantum confinement in CdSe QDs towards the HOMO of the ZnS nanolayer. This is also demonstrated by the fact that the PL peak wavelength does not have varation until 5 layer of ZnS deposited, which also correspond with the absorption measurements reported in Figure S4. It is also interesting to note that the transition between 2 and 5 layers of ZnS correspond to the size of 1 nm and 2.4 nm (determined by ellipsometry) in which the ZnS stops to be quantum confined (bohr radius of ZnS is about 2.5 nm[33]).

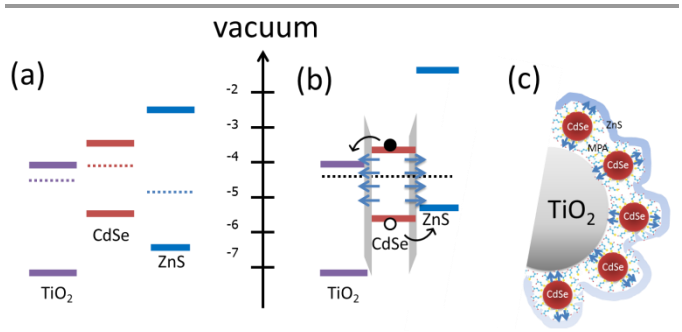

Figure 7. Schemes of the proposed band diagram of the components of the CdSe QD sensitized electrodes (a) before, and (b) after assembly. (c) Cartoon showing the structure of TiO_2/CdSe/ZnS photoelectrodes.

The impact of ZnS coating is also investigated by impedance spectroscopy. The details of these experiments are reported in the supplementary information. Briefly, the charge injection (separation) efficiency (Φ_{inj}) and charge collection efficiency (η_c) can be derived according to equation (1).

$$IQE = \Phi_{inj}.\eta_c \quad (1)$$

Since the EQE measurement was done under weak light intensity (~1mW/cm^2), Figure S8c indicates that the charge collection efficiencies (η_c) of both devices under low light intensity are approaching 100%; therefore, the Φ_{inj} can be estimated to have the same value as the IQE shown in Figure 3. The main reason for the enhanced performance of the samples coated with ZnS is the increased charge injection efficiency. It is important to underline that the impedance spectroscopy, the optical measurements and the electrical measurements performed on the device point to the same interpretation of the role of the ZnS in our device architecture; namely, TiO_2/CdSe and the CdSe/ZnS heterojunctions drive the charge separation upon illumination.

4. Conclusions

We demonstrate highly efficient water splitting and sensitized solar cells by direct adsorption of colloidal CdSe QDs on mesoporous TiO_2 followed by 3-mercaptopropionic acid ligands exchange. The QDSSC with 5L ZnS coating shows the best performance with internal quantum efficiency approaching 100% and energy conversion efficiency over 2%, while for photoelectrochemical H_2 generation the current of ~10 mA/cm^2 under -0.5 V vs SCE was achieved with the same electrode. Moreover, by correlating results from different experimental techniques we explain the role of the ZnS coating in the improved performance of the photo-electrode. Time-resolved photoluminescence indicates the formation of a type II heterojunction in CdSe/ZnS QDs, which together with the other type 2 heterojunction formed with the TiO_2 allows a more efficient carrier separation. Carrier dynamic measurements performed with impedance spectroscopy indicate that the enhanced efficiency of the device with ZnS coating is caused by the higher carrier injection efficiency. Finally, the device results, the impedance spectroscopy, and the optical measurements all point to the same interpretation of the role of the ZnS in our device architecture.

Acknowledgements

Financial support from Foundation for Fundamental Research on Matter (FOM) for the project "Towards bio-solar cells" (FOM15) and the Zernike Institute for Advanced Materials is acknowledged. The authors thank A. Kamp, R. Gooijaarts, and J. Baas for technical support. Finally, the authors would like to thank W. P. Liao, M. C. Chang and Dr. S. Z. Bisri for discussion. L. H. Lai would like to thank Delta Electronics for the support.

Notes and references

[a] Zernike Institute for Advanced Materials, University of Groningen, Nijenborgh 4, Groningen, 9747 AG, The Netherlands.
[b] Department of Chemistry and Applied Biosciences, ETH Zürich, Wolfgang-Pauli-Str. 10, Zurich, 8093, Switzerland.
[c] EMPA-Swiss Federal Laboratories for Materials Science and Technology, Überlandstrasse 129, Dübendorf, 8600, Switzerland.
*E-mail: M.A.Loi@rug.nl. Tel: +31 50 363 4119, Fax: +31 50363 8751.
‡ These authors contributed equally to this work.
† Electronic Supplementary Information (ESI) available: electrochemical reaction in photoanodes and cathodes, the effects of MPA ligand exchange for QDSSCs, absorbance, transmittance and reflectance spectra, photoluminescence of samples with different sequence of CdSe and ZnS on TiO_2, electrochemical impedance spectroscopy (EIS) measurements, equivalent circuit fitting results of EIS and other parameters of cells, and TRPL fitting results. See DOI: 10.1039/b000000x/

1. A. Fujishima and K. Honda, *Nature*, 1972, 238, 37-38.
2. S. Hoang, S. Guo, N. T. Hahn, A. J. Bard and C. B. Mullins, *Nano letters*, 2012, 12, 26-32.
3. M. Batzill, E. Morales and U. Diebold, *Physical Review Letters*, 2006, 96, 026103.
4. J. Luo, L. Ma, T. He, C. F. Ng, S. Wang, H. Sun and H. J. Fan, *The Journal of Physical Chemistry C*, 2012, 116, 11956-11963.
5. J. Luo, S. K. Karuturi, L. Liu, L. T. Su, A. I. Tok and H. J. Fan, *Scientific reports*, 2012, 2, 451.
6. J. Hensel, G. Wang, Y. Li and J. Z. Zhang, *Nano letters*, 2010, 10, 478-483.
7. R. Trevisan, P. Rodenas, V. Gonzalez-Pedro, C. Sima, R. S. Sanchez, E. M. Barea, I. Mora-Sero, F. Fabregat-Santiago and S. Gimenez, *The Journal of Physical Chemistry Letters*, 2013, 4, 141-146.
8. J. W. Lee, D. Y. Son, T. K. Ahn, H. W. Shin, I. Y. Kim, S. J. Hwang, M. J. Ko, S. Sul, H. Han and N. G. Park, *Scientific reports*, 2013, 3, 1050.
9. H. Kim, M. Seol, J. Lee and K. Yong, *The Journal of Physical Chemistry C*, 2011, 115, 25429-25436.
10. P. Rodenas, T. Song, P. Sudhagar, G. Marzari, H. Han, L. Badia-Bou, S. Gimenez, F. Fabregat-Santiago, I. Mora-Sero, J. Bisquert, U. Paik and Y. S. Kang, *Advanced Energy Materials*, 2013, 3, 176-182.
11. K. Shin, S. I. Seok, S. H. Im and J. H. Park, *Chemical communications*, 2010, 46, 2385-2387.
12. H. M. Chen, C. K. Chen, Y. C. Chang, C. W. Tsai, R. S. Liu, S. F. Hu, W. S. Chang and K. H. Chen, *Angewandte Chemie*, 2010, 49, 5966-5969.

13. T. Nann, S. K. Ibrahim, P. M. Woi, S. Xu, J. Ziegler and C. J. Pickett, *Angewandte Chemie*, 2010, 49, 1574-1577.
14. Pan Zhenxiao, ZhaoKe, Wang Jin, Zhang Hua, Feng Yaoyu and Z. Xinhua, *ACS Nano*, 2013, 7, 5215-5222..
15. Y.-L. Lee, C.-F. Chi and S.-Y. Liau, *Chemistry of Materials*, 2010, 22, 922-927.
16. G. Wang, X. Yang, F. Qian, J. Z. Zhang and Y. Li, *Nano letters*, 2010, 10, 1088-1092.
17. M. Seol, J.-W. Jang, S. Cho, J. S. Lee and K. Yong, *Chemistry of Materials*, 2013, 25, 184-189.
18. L. H. Lai, L. Protesescu, M. V. Kovalenko and M. A. Loi, *Physical chemistry chemical physics : PCCP*, 2013, 16, 736-742.
19. A. Salant, M. Shalom, I. Hod, A. Faust, A. Zaban, and U. Banin, *ACS Nano*, 2010, 4, 5962–5968.
20. A. Salant, M. Shalom, Z. Tachan, S. Buhbut, A. Zaban and U. Banin, *Nano letters*, 2012, 12, 2095-2100.
21. X. Y. Yu, J. Y. Liao, K. Q. Qiu, D. B. Kuang and C. Y. Su, *Acs Nano*, 2011, 5, 9494-9500.
22. K.-H. Lin, C.-Y. Chuang, Y.-Y. Lee, F.-C. Li, Y.-M. Chang, I. P. Liu, S.-C. Chou and Y.-L. Lee, *The Journal of Physical Chemistry C*, 2012, 116, 1550-1555.
23. O. Chen, X. Chen, Y. Yang, J. Lynch, H. Wu, J. Zhuang and Y. C. Cao, *Angewandte Chemie-International Edition*, 2008, 47, 8638-8641.
24. N. Guijarro, J. M. Campina, Q. Shen, T. Toyoda, T. Lana-Villarreal and R. Gomez, *Physical chemistry chemical physics : PCCP*, 2011, 13, 12024-12032.
25. S.-m. Yang, C.-h. Huang, J. Zhai, Z.-s. Wang and L. Jiang, *Journal of Materials Chemistry*, 2002, 12, 1459-1464.
26. L. J. Diguna, Q. Shen, J. Kobayashi and T. Toyoda, *Applied Physics Letters*, 2007, 91, 023116.
27. Y.-L. Lee and Y.-S. Lo, *Advanced Functional Materials*, 2009, 19, 604-609.
28. X. Wang, R. Liu, T. Wang, B. Wang, Y. Xu and H. Wang, *ACS applied materials & interfaces*, 2013, 5, 3312-3316.
29. M. Soreni-Harari, N. Yaacobi-Gross, D. Steiner, A. Aharoni, U. Banin, O. Millo and N. Tessler, *Nano letters*, 2008, 8, 678-684.
30. M. Shalom, S. Ruhle, I. Hod, S. Yahav and A. Zaban, *J Am Chem Soc*, 2009, 131, 9876-9877.
31. J. S. Lee, M. V. Kovalenko, J. Huang, D. S. Chung and D. V. Talapin, *Nature nanotechnology*, 2011, 6, 348-352.
32. O. K. Echendu, A. R. Weerasinghe, D. G. Diso, F. Fauzi and I. M. Dharmadasa, *Journal of Electronic Materials*, 2013, 42, 692-700.
33. B. Bhattacharjee, D. Ganguli, K. IakoubovskIi, A. Stesmans and S. Chaudhuri, *Bulletin of Materials Science*, 2002, 25, 175-180.